Journal of Nuclear Materials 406 (2010) 91–96

Contents lists available at ScienceDirect

Journal of Nuclear Materials

journal homepage: www.elsevier.com/locate/jnucmat

Towards a modelling of RPV steel brittle fracture using crystal plasticity computations on polycrystalline aggregates

L. Vincent [a], M. Libert [a,b], B. Marini [a,*], C. Rey [b]

[a] Service de Recherches Métallurgiques Appliquées, CEA, DEN, 91191 Gif-sur-Yvette, France
[b] Laboratoire de Mécanique des Sols, Structures et Matériaux, CNRS, UMR 8579, Ecole Centrale Paris, 92295 Châtenay-Malabry, France

A B S T R A C T

In the frame of the multi-scale approach of the fracture toughness prediction defined in the PERFECT project, we proposed a new crystal plasticity model and applied it to the computation of stress heterogeneities within a reference polycrystalline aggregate defined in the project RPV material.

The proposed crystal plasticity model is able to take into account the effects of temperature and irradiation hardening. The analysis of the results of aggregate computations shows that the distributions of the maximum values of the maximal principal stresses are found to be well described by a Gumbell function. Applying these distributions on a Griffith criterion allows settling the basis of an original fracture criterion. However the increasing resistance to fracture of the steel with temperature can be reproduced only by introducing a temperature dependence of the fracture energy.

1. Introduction

Reactor pressure vessel (RPV) steels of nuclear power plant (A508Cl3, 16MND5, etc.) show strong temperature dependence of the fracture toughness in the range of the Ductile to Brittle Transition Temperature (DBTT) [1]. Starting from values below 0 °C, the transition temperature is increasing during the life of the nuclear plant due to neutron irradiation embrittlement. This behaviour is of great importance for the integrity assessment of the pressure vessel in accidental conditions. As a matter of fact, a convincing demonstration that the onset of brittle fracture cannot be reached in such conditions must be proposed. Toughness data and their scattering can be accurately described in the whole transition, thanks to fracture modellings based on local approach models like Beremin or WST models [2,3]. But in order to reproduce the fast increase of toughness with temperature in the DBTT region, the macroscopic critical cleavage stress must be assumed to be an increasing function of the temperature with a dependence on neutron irradiation [4–6]. In iron, experiments reveal that the surface energy γ_s (J/m^2) which is related to the cleavage stress is fairly independent of temperature [7,8]. For bainitic steels, it is experimentally found that the macroscopic critical cleavage stress is almost temperature independent, at least, in the lower shelf of the fracture toughness [9]. Therefore, the use of a temperature-dependent macroscopic critical cleavage stress in computations needs to be rationalized through a multi-scale physical approach [10]. Starting from dislocation behaviour, this multi-scale approach has to account for many different scales [11]. One of them is the polycrystalline aggregate which links the collective behaviour of dislocations with the macroscopic behaviour. In this attempt to predict the brittle fracture which is controlled by the largest values of the stresses, a precise computation of the stress distributions in the aggregate is mandatory. Of course, this requires, in the first place, a precise behaviour law to capture the local stress amplification due to the local crystal disorientations. The objective of this paper is to present the application of this modelling to unirradiated and then irradiated RPV steel.

2. Material

The RPV material used in this study is the main reference material of the PERFECT project named Euromaterial A. It is a 22NiMoCr37 type steel (German standard).

The material is used in the quenched and tempered condition. For quenching, the forging has been heated up in steps to 880 °C, then held at this temperature for 8 h and finally quenched. Afterwards it has been heat treated at 660 °C for 8 h and cooled down in air to room temperature (see Table 1).

Specimens were neutron irradiated in the VAK reactor by Areva Gmbh. The fluence is 4.3×10^{19} n/cm^2 with a neutron energy $E_n > 1$ MeV. The material properties were characterized by tensile testing in irradiated and unirradiated conditions. The hardening of the material is observed on the yield stress and on the ultimate tensile stress. Ductility characteristics do not show significant evolution (Table 2).

* Corresponding author. Tel.: +33 (0) 169088599; fax: +33 (0) 169087167.
E-mail address: bernard.marini@cea.fr (B. Marini).

0022-3115/$ - see front matter © 2010 Elsevier B.V. All rights reserved.
doi:10.1016/j.jnucmat.2010.07.022

Table 1
Chemical composition of the Euromaterial A in wt.%. (*Source*: AREVA NP Gmbh.)

C	Si	P	S	Cr	Mn	Ni	Cu	Mo	Ti	V	Nb	Al	Fe
0.22	0.23	0.007	0.004	0.39	0.88	0.84	0.08	0.51	0.001	0.003	<0.005	0.013	Bal.

Table 2
Conventional tensile properties at room temperature. (*Source*: AREVA NP Gmbh.)

Condition	T (°C)	Yield stress (MPa)	Ultimate tensile stress (MPa)	Total elongation (%)	Reduction of area (%)
Unirradiated	25	464	602	24	72
Irradiated	25	540	818	26	65

3. Crystal plasticity modelling

Within the framework of the classical theory of thermally activated dislocation motion, a unified constitutive description of the mechanical behaviour for bcc material was developed in the frame of a PhD thesis [12,13]. The model accounts for crystallographic glide and resulting lattice rotation. For bcc structure, glide is assumed to occur on the 24 $\{1\,1\,0\}\langle 1\,1\,1\rangle$ and $\{1\,1\,2\}\langle 1\,1\,1\rangle$ slip systems. Most of the bcc structures exhibit a transition in terms of plasticity mechanisms. At low temperature and up to room temperature, plasticity is governed by the thermally activated mobility of the screw dislocations (double kink mechanism). At higher temperatures, plasticity also depends on forest hardening. So, the selected viscoplastic constitutive behaviour must describe the competition between lattice friction and forest hardening. This crystal plasticity model is composed of three main contributions [14,15]:

Plastic flow law (the superscript s denotes the considered slip system) [16]:

$$\dot{\gamma}^s = \dot{\gamma}_0 \exp\left[-\frac{\Delta G\left(\tau^s_{eff}\right)}{k_B T}\right] \tag{1}$$

With $\dot{\gamma}^s$ the plastic slip glide rate, $\dot{\gamma}_0$ a material dependant parameter, k_B the Boltzmann's constant and T the absolute temperature. τ_{eff} is the effective shear stress acting on the slip system s, which can be seen as the driving force of the thermal activated mechanisms. The activation enthalpy ΔG is given by the expression [17,18]:

$$\Delta G(\tau^s_{eff}) = \Delta G_0\left(1 - \left(\frac{\tau^s_{eff}}{\tau_p}\right)^p\right)^q \tag{2}$$

where τ_p, p and q are material dependant parameters.

Hardening law [19,20]:

$$\tau^s = \tau_0 + \tau_\mu + \tau_{eff} \tag{3}$$

With

$$\tau^s_\mu = \frac{(\mu b)^2 \sum_u a^{su}\rho^u}{\tau^s - \tau_0} \tag{4}$$

τ_0 is the initial critical shear stress and $\tau\mu$ is the "athermal" stress due to the long range obstacles, here the forest dislocations. μ is the isotropic shear modulus and a^{su} are the coefficients of the slip systems interaction matrix [19,20].

It should be noted that τ_0 is not the same for $\{1\,1\,0\}$ and $\{1\,1\,2\}$ slip systems [12,13]:

$$\tau_0^{\{1\,1\,2\}} = \tau_0^{\{1\,1\,0\}} + f(T) \quad \text{with } f(T) = -0.357T + 73.7 \quad \text{for } T < Tc$$
$$= 206\ ^\circ\text{K} \quad \text{and } f(T) = 0 \text{ for } T > Tc.$$

Dislocation density evolution law [21]:

$$\dot{\rho}^s = \frac{|\dot{\gamma}^s|}{b}\left(\frac{1}{\Lambda^s} - g_c(T)\rho^s\right) \tag{5}$$

with b the norm of Burger's vector and Λ^s, the mean free path, dependant on both the forest density and the average "bainitic block" size d:

$$\frac{1}{\Lambda^s} = \frac{1}{d} + \frac{\sqrt{\sum_{u\neq s}\rho^u}}{K(T)} \tag{6}$$

with $K(T)$ a material parameter dependant on temperature.

The annihilation distance is assumed to be a thermally activated according to:

$$g_c(T) = g_{c0}\exp\left[-\frac{E_{gc}}{k_B T}\right] \tag{7}$$

where g_{c0} and E_{gc} are two different material dependant parameters.

This model was implemented with an implicit integration scheme in the CAST3M finite element code [22] in the framework of finite strain.

The identification of most material parameters was made in a previous work for a bainitic steel [12]. In this paper, only two material parameters, namely τ_0 and $K(T)$, are re-evaluated on Euromaterial A for a solution annealed and an irradiated state. In addition, it is assumed that first, all other material parameters should stay constant from a bainitic steel to another and second, that irradiation only changes the initial critical shear stress τ_0 and the mean free path of the dislocations.

For the evaluation purpose, tensile test simulations are realized with a simplified aggregate of $15\times15\times15$ quadratic finite elements with a random crystalline orientation for each finite element. The optimized values of the material parameters are obtained with the SiDoLo software [23] by minimizing the difference between experimental results and the macroscopic response of the polycrystalline Finite Element computations. The experimental data base contains results for two temperatures on the unirradiated material and two different temperatures on the irradiated state.

The optimum set of parameters is given in Tables 3a–3c and the comparison between experimental and simulation results are plotted in Fig. 1. As expected, irradiation increases the "friction" stress τ_0. The parameter K appears to be temperature dependant but not irradiation dependant.

Table 3a
Parameters of the plastic flow law.

$\dot{\gamma}0$ (s^{-1})	ΔG_0 (eV)	τ_R (MPa)	p	q
10^6	1.00	498	0.283	1.17

Table 3b
Parameters of the hardening law.

τ_0 (MPa)		a^{su}
Unirradiated	Irradiated	
37.4	72	0.251

Table 3c
Parameters of the dislocation density evolution law.

ρ_0 (m^{-2})	g_{c0} (nm)	E_{gc} (eV)	K			
			Unirradiated		Irradiated	
			−90 °C	−50 °C	−120 °C	−50 °C
10^{14}	18.6	2.17×10^{-2}	65.9	44.5	110	43.4

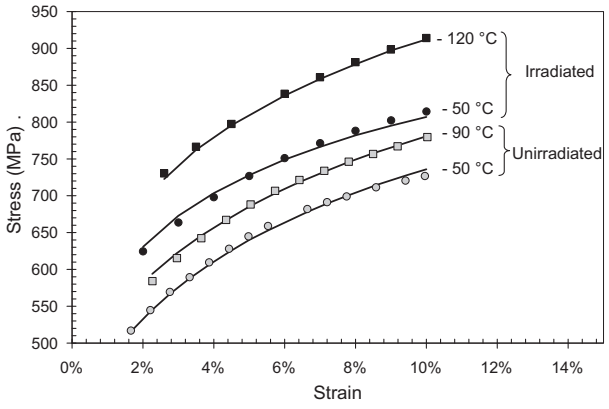

Fig. 1. Parameterization of the model using four tensile tests results on Euromaterial A: solid lines represent the simulation results and closed symbols the experimental data.

4. Aggregate simulations

The constitutive equations are now used in finite element computations of aggregates with special boundary conditions assuring an approximately constant stress triaxiality ratio of 2.5 under plane strain state. These mechanical conditions are assumed to be representative of those found in the process region of a crack tip. The finite element mesh of the aggregate is built from an EBSD map plotted in Fig. 2. The size of each finite element is V_{el} = $1 \times 1 \times 1$ μm^3.

Finite element method computations are performed with the crystal plasticity model and for the four identification conditions of the material parameters presented previously. The results are post-treated in order to study the stress distributions and in particular, the maximum principal stress distributions since these results are used to predict the onset of brittle fracture (Fig. 3). In a sense, it is here assumed that the finite element simulations that are run on only one type of large aggregate give access to the same distribution of extreme values than the distribution that would be obtained with several simulations on different small aggregates (with different shape and crystallographic orientations for the grains constituting such small aggregates). This last way of obtaining distribution of extreme values will be followed in a future work.

The stress field is averaged inside each element prior to generating the stress distributions. The stress distributions correspond thus to the distributions of mean stresses over a 1 μm^3 elementary volume. The most useful part in these distributions corresponds to the highest values, which are described using a Gumble type function for simplicity. Other functions could have been used (Weibull

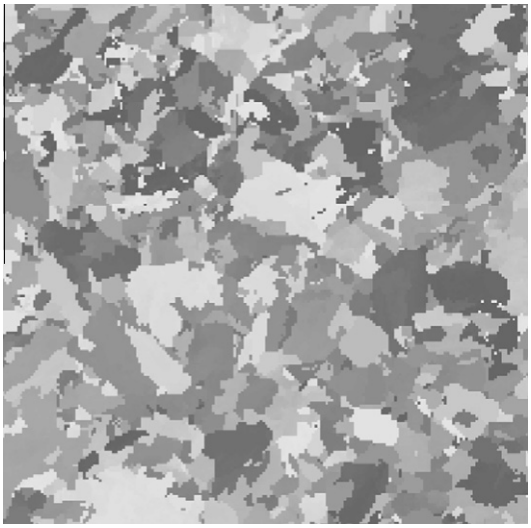

Fig. 2. EBSD map of a 200×200 μm^2 aggregate of Euromaterial A used to construct the FE polycrystalline mesh. The grey levels correspond to different values of the first Euler angle (ϕ_1). (*Source*: VTT).

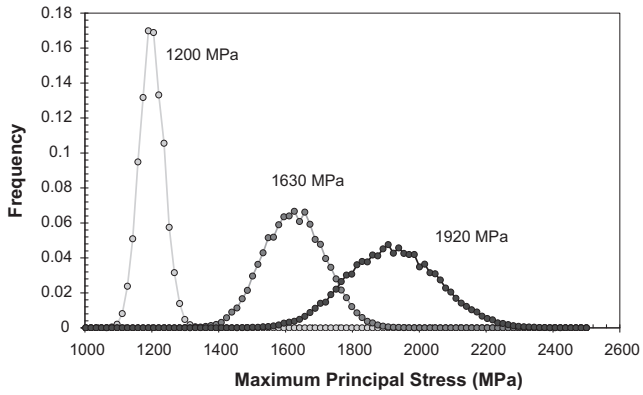

Fig. 3. Example of a distribution of the maximum principal stresses inside the aggregate for three average maximum principal stresses: 1200, 1630 and 1920 MPa (unirradiated material at −50 °C).

for instance) but it happened that the Gumbel function correctly matched the numerical distributions obtained from aggregate simulations.

And so, the probability to find a maximum principal stress higher than a given value σ_I in one finite element out of a polycrystalline aggregate submitted to an average maximum principal stress $\langle\sigma_I\rangle$ and an average von Mises stress $\langle\sigma_{\text{Mises}}\rangle$ can be expressed as:

$$P(\sigma^* > \sigma_I) = 1 - \exp\left(-\exp\left(-\left(\frac{\sigma_I - \langle\sigma_I\rangle}{\alpha_1\langle\sigma_{Mises}\rangle + \beta_1} + \gamma_1\right)\right)\right) \quad (8)$$

The identified values of α_1, β_1 and γ_1 are presented in Table 4. Fig. 4 shows three fittings of the extreme values of the stress distribution according to Eq. (8) and for three levels of the mean principal axial stress. The fittings only consider cumulative probabilities above 90%. The denominator of Eq. (8) is responsible for the scatter of the distribution. This scatter appeared to be a non-linear increasing function of the amount of macroscopic plastic strain [12] relatively independent of the temperature and of the stress triaxiality ratio. However, even though this relation seemed promising, very few high values of macroscopic plastic strain could be used to identify such a non-linear relation. Moreover, some discrepancies did not allow to have a confident estimation for this function [12]. Finally, it

Table 4
Parameter values for the distributions of the maximum principal stresses.

Condition	Temperature (°C)	α_1	β_1	γ_1
Unirradiated	−90	0.105	−25.16	1.26
	−50	0.126	−38.463	1.40
Irradiated	−120	0.142	−64.64	1.19
	−50	0.125	−44.59	1.36

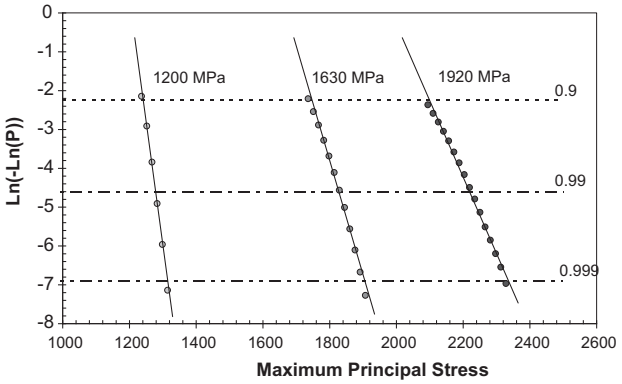

Fig. 4. Fit of the extreme values for three average maximum principal stresses: 1200, 1630 and 1920 MPa (unirradiated material at −50 °C).

happened that a linear function of the macroscopic von Mises equivalent stress with temperature dependant parameters was better suited to fit numerical data. The type of distribution function (Gumbel) and of the variables used to feed this function is not definitive and more general work on this matter should be realized.

5. Towards the modelling of brittle fracture

The ultimate goal of the present modelling is the prediction of brittle fracture at different temperature and irradiation conditions. The proposed model is based on a rough description of cleavage fracture: in a representative volume V_0, micro-cracks initiate for a certain level of plastic strain and then propagates when a local stress reaches a critical value. These assumptions are similar to those of the Beremin model [2] albeit heterogeneous stress (due to the microstructure) is used instead of an averaged stress, using the data from finite element method computations.

The fracture stress σ_f of the volume V_{el} (typically 1 μm^3) is the stress needed to overcome propagation barriers, like the carbides–matrix interfaces. This quantity is given by a Griffith type criterion:

$$\sigma_f = \sqrt{\lambda \frac{E.\gamma_f}{r}} \tag{9}$$

where λ is a micro-crack shape factor, E the Young modulus, γ_f the fracture surface energy and r is the size of the micro-defect which becomes instable (i.e. propagates) under the local stress σ_f . In the following, we will take $\gamma_f = 8$ J/m^2.

If we assume that the micro-cracks are mainly produced by the cracking of the carbides or of their interface with the ferritic matrix, we can approximate the size of the micro-cracks to the carbides size. Using Eqs. (8) and (9), it is possible to compute the probability of an average sized carbide to be at the origin of the brittle fracture in a given aggregate, as a function of the average maximum principal stress.

In the real material, the carbide size is distributed. This distribution has been measured on bainitic steels by Lee et al. in 2002 [24]. They proposed the following probability function for the carbides radii (in μm):

$$F(r) = P(r < r_0) = 1 - \exp\left(-\left(\frac{2r_0 - 0.00917}{0.10158}\right)^{1.192}\right) \tag{10}$$

To take into account this distribution of carbide sizes, we propose to compute the probability of failure of carbide by integrating the probability density of the carbide size weighted by the probability that the local stress will be higher than the fracture stress which is a function of the size (Eq. (9)). So the probability of failure of volume v containing 1 carbide embedded in an aggregate under the macroscopic loading Σ is written:

$$P_f(v, \Sigma) = \int_0^{+\infty} \frac{dF(r)}{dr} P(\sigma_I(\Sigma) > \sigma_f(r)) dr \tag{11}$$

The term under the integral symbol in Eq. (11) is graphically presented in Fig. 5. It can be observed that the curve portion above the critical carbide diameter corresponds to the classical Beremin term (Eq. (9)) whereas the curve portion below this value corresponds to the amplification effect, induced by the microstructure. This new part named the "aggregate" effect, which is a function of the macroscopic loading (i.e. maximum principal stress and triaxiality) and of temperature.

To compute the probability of failure of a representative volume V_0, we have to account for the number of carbides N present in this volume, which is the product of the number density of carbide n_c with V_0. In the following, we choose $V_0 = (50\ \mu m)^3$ and $n_c = 0.76\ \mu m^{-3}$ [25].

We now make the assumption that the weakest link theory could be used to describe the fracture of the volume V_0. This means that we assume a failure of the representative volume V_0 is due to the first instable micro-crack i.e. there is no micro-crack arrest. In this condition the probability of non-fracture of V_0 is the product of the probabilities of non-fracture of the N volume elements v of V_0 containing one carbide particle.

$$1 - P_f(V_0, \Sigma) = \prod_{v \in V_0} (1 - P_f(v, \Sigma)) = (1 - P_f(v, \Sigma))^{n_c V_0} \tag{12}$$

If we now consider a macroscopic plastic zone of volume V_p containing a large number of volumes V_0, the macroscopic probability of failure could be written again from the application of the weakest link and the previous equation can be rewritten into a continuous form. Considering Eq. (10), the general form of the probability of failure is

$$P_f(V_p) = 1 - \exp\left(\int_{V_0 \in V_p} \ln\left(1 - \left(\int_0^{+\infty} \frac{dF(r)}{dr} P(\sigma_I(\Sigma(V_0)) > \sigma_f(r)) dr\right)\right)^{n_c V_0} dV\right) \tag{13}$$

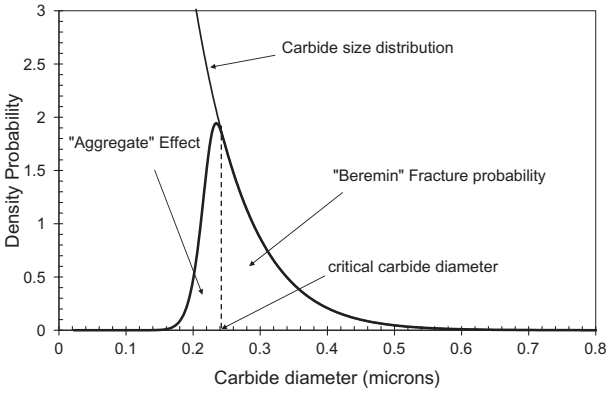

Fig. 5. Probability density function as a function of the carbide size, for an applied stress corresponding to a 10% probability of fracture of one carbide particle.

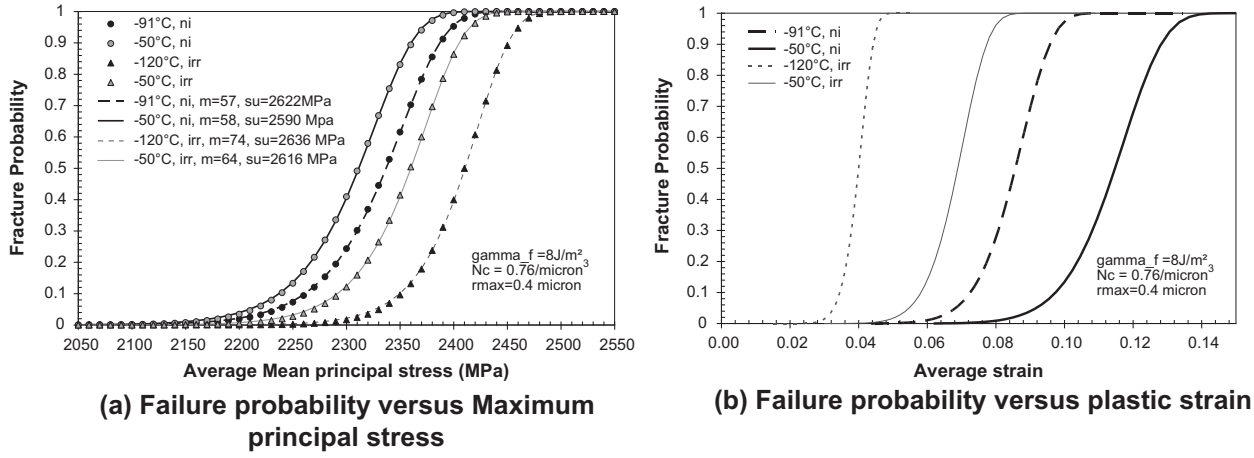

Fig. 6. Failure probability of a CT25 for two temperatures and two irradiation states and a constant fracture surface energy. The identified Weibull parameters apply to the representative volume element $V_0 = (50\ \mu m)^3$.

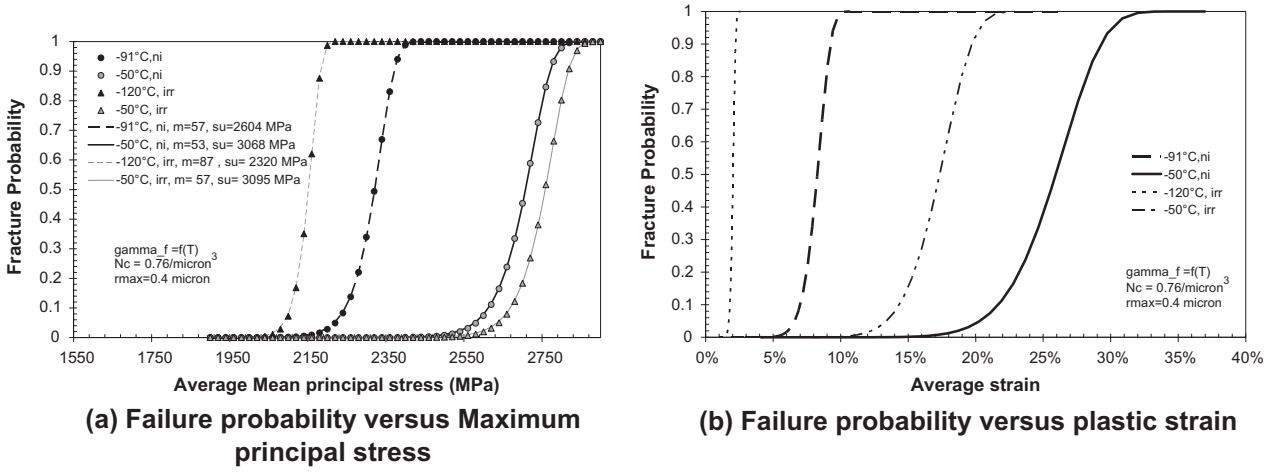

Fig. 7. Failure probability of a CT25 for two temperatures and two irradiation states. Fracture surface energy function of the Temperature. The identified Weibull parameters concern the representative volume element $V_0 = (50\ \mu m)^3$.

It is possible to incorporate in this equation the analytical expressions of the density of the carbide size distribution and of the distribution of the extreme values of the maximum principal stresses [12].

The present model can be considered as an extension of the Beremin model [2] incorporating an explicit dependence on the stress state and plastic strain (Eq. (8)).

A tentative evaluation of the fracture probability of CT25 type specimen is performed with the above-described brittle fracture model. The onset of brittle fracture is assumed to occur in the first row of elements located at the crack tip. We consider that these elements have a volume equal to $V_0 = (50\ \mu m)^3$ and that they are all submitted to the same stress state with a constant stress triaxiality ratio of 2.5. Under these conditions, Eq. (13) becomes:

$$P_f(CT_{25}) = 1 - \left(1 - \left(\int_0^{+\infty} \frac{dF(r)}{dr} P(\sigma_I(\Sigma(V_0)) > \sigma_f(r))dr\right)\right)^{\frac{25}{0.05}\eta_c V_0} \quad (14)$$

In Fig. 6a, the failure probabilities versus the maximum principal stress are plotted considering a constant fracture surface energy γ_f equal to 8 J/m^2 and the distribution of carbide sizes reported in Eq. (10) with a maximum particle diameter of 0.4 μm.

For a given fracture probability, the average maximum principal stress decreases with temperature. Moreover, for a fixed temperature and fracture probability, the average maximum principal stress is larger for the irradiated state than for the annealed state. These two findings are a priori in contradiction with the expected, experimental results. In fact, the curves in Fig. 6 shows that plasticity is more developed at higher temperature for the same average macroscopic stress state and therefore, a more heterogeneous stress state is present in the polycrystal. The direct consequence of this result is that, for a given mean stress, it is easier to find a local stress larger than a given critical stress when the temperature is larger. Accordingly, the irradiated state leads to a stiffer behaviour and thus, for a given macroscopic stress state, plasticity is limited by the irradiation as well as the heterogeneity of the stress field in the aggregates. Therefore it is more difficult to find a stress larger than a critical stress after irradiation.

However, the modelling results become consistent with the experiments if the fracture probability is expressed as un function of the average plastic strain (Fig. 6b) since, this time, the average plastic strain for a given failure probability increases with temperature and decreases with an augmenting irradiation dose. In other words, for a given failure probability, increasing the irradiation, dose and decreasing the temperature yield the same effect: to diminish the ductility of the material.

Another result of the model is the effect of stress triaxiality. As a matter of fact, for a given fracture probability, the higher the stress triaxiality, the larger the average mean principal stress and the smaller average plastic strain.

We now assume that the fracture surface energy is an increasing function of temperature. In Fig. 7, the fracture probabilities are calculated again considering this time that the "apparent" fracture energy surface [26]:

$$\gamma_f(T) = 1.53\exp(0.009(T + 273.15)) \quad (15)$$

In this case, the fracture probability curves versus the average maximal principal stress describe the expected effects. For a given fracture probability indeed, an increasing temperature produces an increase of the average maximal principal stress. Moreover, an increasing irradiation dose reduces the average maximal principal stress associated with a given fracture probability.

Due to the increase of γ_f with the temperature, the above-described effects of temperature and irradiation on the fracture ductility are even more pronounced (Fig. 7b).

Down to -50 °C and for a given fracture probability, the average maximum principal stress remains higher in the irradiated state than in the annealed state (even if the fracture ductility is higher for the annealed state). This effect might comes from the irradiation changes the magnitude of the "apparent" fracture surface energy, which has not been taken into account in the present work.

6. Conclusions

In the frame of the multi-scale approach of the fracture toughness prediction defined in the PERFECT project, we have proposed a new crystal plasticity model and applied it to the computation of the heterogeneity of stresses inside a reference polycrystalline aggregate, defined in the RPV material project. The following conclusions have been presented:

- The proposed crystal plasticity model is able to take into account the effect of temperature and the effect of irradiation hardening with the modification of two key parameters: respectively the parameter controlling the dislocations multiplication and the critical resolved shear stress.
- The maximum values of the maximal principal stresses are accurately described by a Gumbell function.
- The study of the different computed fracture stress distributions shows an influence of the irradiation and of the temperature on the average fracture stress and its scatter.
- The basis of an original local approach model taking into account the stress heterogeneities induced by the microstructure are proposed.

The ongoing work on this modelling is concerned with the improvement of the crystal plasticity model to explicitly account for irradiation damage defects. The next step in fracture modelling is to introduce the model in a finite elements code and validate it on fracture toughness results. It is a challenging task as it seems that temperature dependence of the apparent surface energy is to be derived from models treating lower scale phenomena [27,28].

References

[1] S. Carassou, S. Renevey, B. Marini, A. Pineau, ECF12 Proceedings Sheffield, vol. 2, 1998, p. 691.
[2] F.M. Beremin, Metall. Trans. A 14A (1983) 2277–2287.
[3] K. Wallin, T. Saario, Törrönen, Metal Sci. 18 (1984) 13–18.
[4] C. Eripret, D. Buisine, G. Rousselier, Seminar for Promotion of Local Approach, Tempere, 1992.
[5] B.Z. Margolin, A.G. Gulenko, V.A. Nikolaev, L.N. Ryadkov, Int. J. Pres. Ves. Pip. 80 (2003) 817–829.
[6] C. Bouchet, B. Tanguy, J. Besson, S. Bugat, Comput. Mater. Sci. 32 (2005) 294–300.
[7] J.J. Gilman, Cleavage, ductility and tenacity in crystals, in: B.L. Averbach, G.T. Hahn, et al. (Eds.), Fracture, New York, 1959, pp. 193–224.
[8] A.T. Price, H.A. Holl, A.P. Greenough, Acta Metall. 12 (1964).
[9] P. Bowen, S.G. Druce, J.F. Knott, Acta Metall. 34 (6) (1986) 1121–1131.
[10] S.G. Roberts, in: Proceedings of the Multiscale Phenomena in Plasticity, Ouranopolis, Greece, 8–19 September, 1999.
[11] D. Lidbury, S. Bugat, O. Diard, E. Keim, B. Marini, H.-W. Viehrig, K. Wallin, in: Proceedings of ASME PVP 2005, Denver, Colorado, July 17–21, 2005.
[12] M. Libert, Doctoral Thesis, Ecole Centrale de Paris, 2007.
[13] M. Libert, C. Rey, L. Vincent., B. Marini, Int. J. Plast., submitted for publication.
[14] D. Peirce, R.J. Aaroet, A. Needleman, Acta Metall. 31 (1983) 1951–1976.
[15] C. Teodosiu, J.L. Raphanel, L. Tabourot, Finite element simulation of the large elastoplastic deformation of multicrystals, in: Teodosiu, Raphanel, Sidoroff (Eds.), MECAMAT'91© Balkema, Rotterdam, 1993, pp. 153–160, ISBN: 90 5410 317 5.
[16] F. Louchet, Plasticité des métaux de structure cubique centrée à basse température: déformation in-situ par microscopie électronique à haute tension. PhD Université Paul Sabatier de Toulouse, 1976.
[17] E. Rauch, Etude de l'écrouissage des métaux, aspects microstructuraux et lois de comportement, HDR, Institut National Polytechnique de Grenoble, 1993.
[18] U.F. Kocks, A.S. Argon, M.F. Ashby, Thermodynamics and kinetics of slip, in: Progress in Materials Science, vol. 19, Pergamon Press, Oxford, 1975.
[19] P. Franciosi, Acta Metall. 31 (9) (1983) 1331–1342.
[20] E. Rauch, Etude de l'écrouissage des métaux, aspects microstructuraux et lois de comportement, Mémoire d'HDR, Institut National Polytechnique de Grenoble, 1993.
[21] Y. Estrin, H. Mecking, Acta Metall. 32 (1) (1984) 57–70.
[22] Cast3m. <http://www.cast3m>.
[23] P. Pilvin, Notice d'utilisation de SiDoLo version 2.4495, Laboratoire de Génie Mécanique et Matériaux, 56321 Lorient, France, Janvier, 2003.
[24] S. Lee, S. Kim, B. Hwang, B.S. Lee, C.G. Lee, Acta Mater. 50 (2002) 4755–4762.
[25] S.R. Ortner, J. Duff, D.W. Beardsmore, Characterisation of Euro A reference steel for application of EOH model of brittle fracture, in: Technical Report SA/EIG/15234/R003 – Project PERFECT, SERCO Assurance.
[26] J.P. Mathieu, Analyse et modélisation micromécanique du comportement et de la rupture fragile de l'acier 16MND5: Prise en compte des hétérogénéités microstructurales, PhD Thesis, ENSAM Metz, 2006.
[27] C. Robertson, K. Obrtlik, B. Marini, J. Nucl. Mater. 366 (2007) 58–69.
[28] J. Chaussidon, C. Robertson, D. Rodney, M. Fivel, Acta Mater. 56 (2008) 5466–5476.